Drug Delivery and Translational Research (2025) 15:4761–4774
https://doi.org/10.1007/s13346-025-01886-w

ORIGINAL ARTICLE

D-mannose augments targeted radioligand-immunotherapy of prostate cancer by enhancing radiosensitivity and reshaping immune microenvironment

Lei Tao[1] · Bin Xu[1] · Juan Sun[1] · Jiangtao Yang[1] · Fenghua Meng[1] · Zhiyuan Zhong[1,2]

Accepted: 19 May 2025 / Published online: 14 June 2025
© Controlled Release Society 2025

Abstract

Targeted radioligand therapy (TRT) is an emerging therapeutic modality for advanced tumors like metastatic castration-resistant prostate cancer. The patients bare, however, varying degrees of resistance to TRT, which would greatly lessen the treatment efficacy and response rate. Here, we find that oral medication of D-mannose effectively enhances the radiosensitivity of PSMA-positive murine RM1-hPSMA prostate cancer cells to TRT by suppressing glucose metabolism. This metabolic disruption not only impeded the proliferation of RM1-hPSMA cells but also augmented DNA damage within tumor cells subjected to TRT, co-promoting cell apoptosis. Interestingly, TRT-D-mannose combination strongly boosted the anti-tumor immune responses by inducing immunogenic cell death, disrupting the immune evasion mechanisms employed by tumor cells, and reducing immunosuppressive cells in the tumor. D-mannose significantly improved the TRT efficacy for highly aggressive murine RM1-hPSMA and human LNCaP Clone FGC models, without causing adverse effects. Hence, D-mannose is potentially a safe radio-sensitizer and a potent immune activator for TRT.

Keywords Targeted radioligand therapy · Radio-sensitizer · Prostate cancer · Immune response · Tumor microenvironment

Introduction

Prostate cancer (PC) ranks as the fifth leading cause of cancer-related mortality among men globally [1]. Within five years after diagnosis, about 20% PC patients will progress to metastatic castration-resistant prostate cancer (mCRPC), a stage that poses significant therapeutic challenges [2, 3]. Targeted radioligand therapy (TRT), which utilizes lutetium-177 (^{177}Lu) as a radionuclide and prostate-specific membrane antigen (PSMA) as a target, offers a breakthrough treatment for mCRPC [4, 5]. Notably, despite its potential to slow down disease progression and extend patient survival time, approximately 30% of patients exhibited resistance to TRT monotherapy [6]. The existing intrinsic and acquired resistance to TRT, which would greatly lessen the treatment efficacy and response rate, is a critical issue for clinical outcomes [7–9].

The glycolytic activity is markedly elevated in mCRPC cells, with characteristics of increased lactate production and ATP generation [10]. The radiation therapy, while effective in killing tumor cells, may inadvertently exacerbate glycolytic processes, reducing tumor cell sensitivity to radiation [11] and promoting immune evasion [12, 13]. Additionally, radiation may activate alternative metabolic pathways, further enhancing tumor cell resistance to treatment [14]. To enhance tumor cell sensitivity to radiation, researchers have proposed strategies to inhibit glycolysis or oxidative phosphorylation, key components of tumor metabolism [15–18]. However, the inhibition of various metabolic pathways in tumor cells may impact the proliferation and functionality of immune cells such as effector T cells and dendritic cells [19–21]. This highlights the need for careful evaluation of metabolic modulation strategies within the context

Lei Tao and Bin Xu have contributed equally to this work.

✉ Fenghua Meng
fhmeng@suda.edu.cn

✉ Zhiyuan Zhong
Zhongzyzhong@suda.edu.cn

[1] Biomedical Polymers Laboratory, College of Chemistry, Chemical Engineering and Materials Science, and State Key Laboratory of Radiation Medicine and Protection, Soochow University, Suzhou 215123, People's Republic of China

[2] College of Pharmaceutical Sciences, Soochow University, Suzhou 215123, People's Republic of China

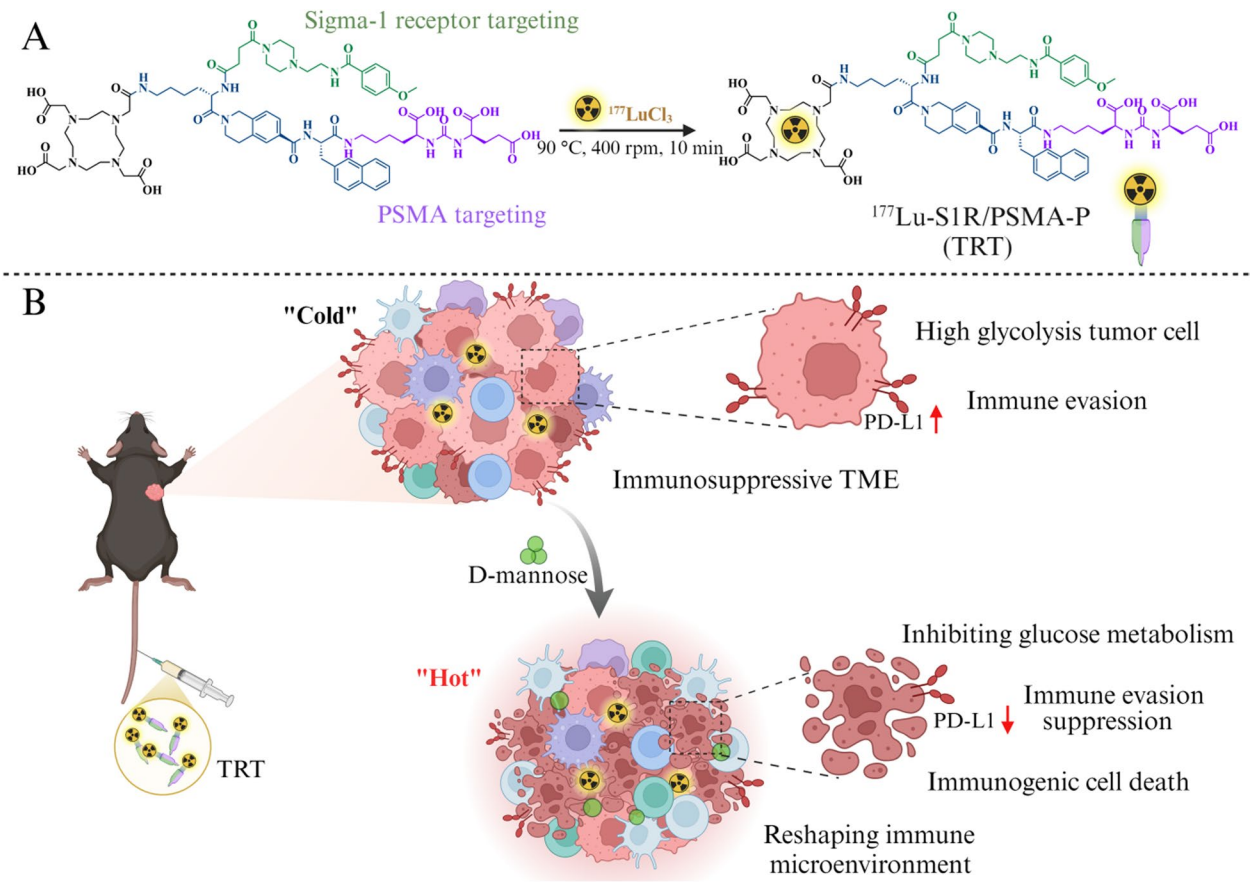

Scheme 1 Schematic illustration of enhanced TRT of prostate cancer by supplementing D-mannose. (**A**) S1R/PSMA-P is a sigma-1 receptor and PSMA dual-targeted radioligand. (**B**) D-mannose enhances the radiosensitivity of PC cells to TRT by suppressing TRT-induced glucose metabolism reprogramming, and improves the anti-tumor immune responses by inducing immunogenic cell death, disrupting the immune evasion mechanisms employed by tumor cells, and reducing immunosuppressive cells in the tumor

of a fully functional immune system. Moreover, given that most malignant cells can switch between various metabolic states to sustain tumor progression [22], targeting a single metabolic pathway may be insufficient to meet therapeutic needs [23]. Recently, D-mannose, a naturally occurring monosaccharide, has garnered attention for its anti-tumor potential [24]. D-mannose could disrupt glycolysis in tumor cells, thereby inhibiting cell growth [25], and mitigate the acidosis induced by high glucose uptake in tumor cells, reducing drug resistance and enhancing chemotherapy [25]. D-mannose was reported to enhance the sensitivity of triple-negative breast cancer cells to radiation by downregulating mRNA levels of DNA repair genes [26]. Furthermore, D-mannose could regulate the tumor microenvironment and enhance anti-tumor immunity in mouse models, showing synergistic effects when combined with immune checkpoint inhibitors [27, 28].

Here, we report on oral administration of D-mannose to enhance the radiosensitivity of PC cells to TRT (Scheme 1). In contrast to external radiation therapy, TRT induces specific and prolonged radiation exposure [29]. We recently developed a dual-targeted radioligand, S1R/PSMA-P, which utilizing ^{177}Lu or ^{225}Ac as a radionuclide showed better therapeutic efficacy for PC than single targeted PSMA-617 [30, 31]. The aim of this study was to investigate the radiosensitizing effect of D-mannose in TRT with ^{177}Lu-S1R/PSMA-P for prostate cancer, with a focus on elucidating the underlying mechanisms by which D-mannose modulates tumor cell metabolism to enhance radiosensitivity and its role in reshaping the tumor immune microenvironment. These insights may contribute to developing interesting strategies to boost TRT and immunotherapy for advanced tumors.

Methods

Radiolabeling

Radiolabeling was performed as our previous report [30] with slight modifications. Briefly, S1R/PSMA-P (0.2 mg)

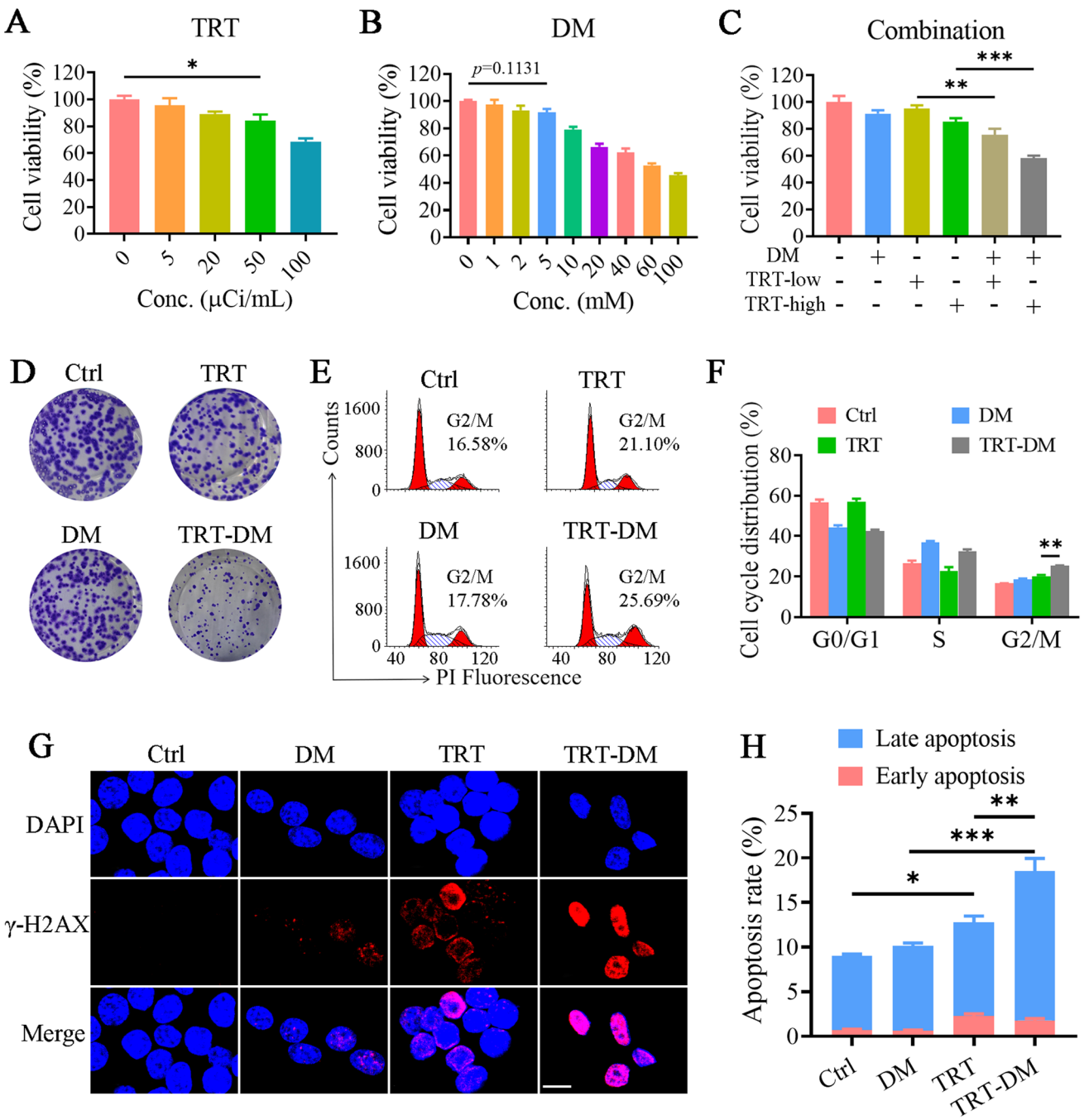

Fig. 1 In vitro sensitizing effects of DM on TRT. Viability of RM1-hPSMA cells incubated with different doses of (**A**) TRT, (**B**) DM or (**C**) TRT (5 or 50 μCi/mL) plus DM (5 mM) for 48 h (n = 6). (**D**) Clone formation assay of RM1-hPSMA cells treated with TRT (50 μCi/mL), DM (5 mM) or TRT-DM for 7 days. (**E**) Cell cycle flow cytometric histogram and (**F**) quantitative analysis of RM1-hPSMA cells under different treatments for 48 h by flow cytometry (TRT: 50 μCi/mL, DM: 5 mM, n = 3). (**G**) Immunofluorescence images of γ-H2AX expression of cells post varous treatments and DAPI staining (scale bar: 10 μm). (**H**) Percentages of apoptotic cells after different treatments (TRT: 50 μCi/mL, DM: 5 mM, n = 3). Data are presented as mean ± SEM. The p values in **A-C**, **F** and **H** were calculated by one-way ANOVA with Tukey's multiple comparison test; * $p < 0.05$, ** $p < 0.01$, *** $p < 0.001$

was dissolved in 200 μL of 0.4 M ascorbic acid buffer (pH 4.5) and sonicated for 5 min. Next, 1 mCi of $^{177}LuCl_3$ was prepared in a 1.5 mL Eppendorf tube. An appropriate volume of the S1R/PSMA-P solution, ensuring a 1:6 molar ratio between ^{177}Lu and DOTA, was added, followed by adding ascorbic acid buffer to achieve a final volume of 50 μL. The mixture was then incubated at 90 ℃ with shaking at 400 rpm for 10 min to complete the reaction.

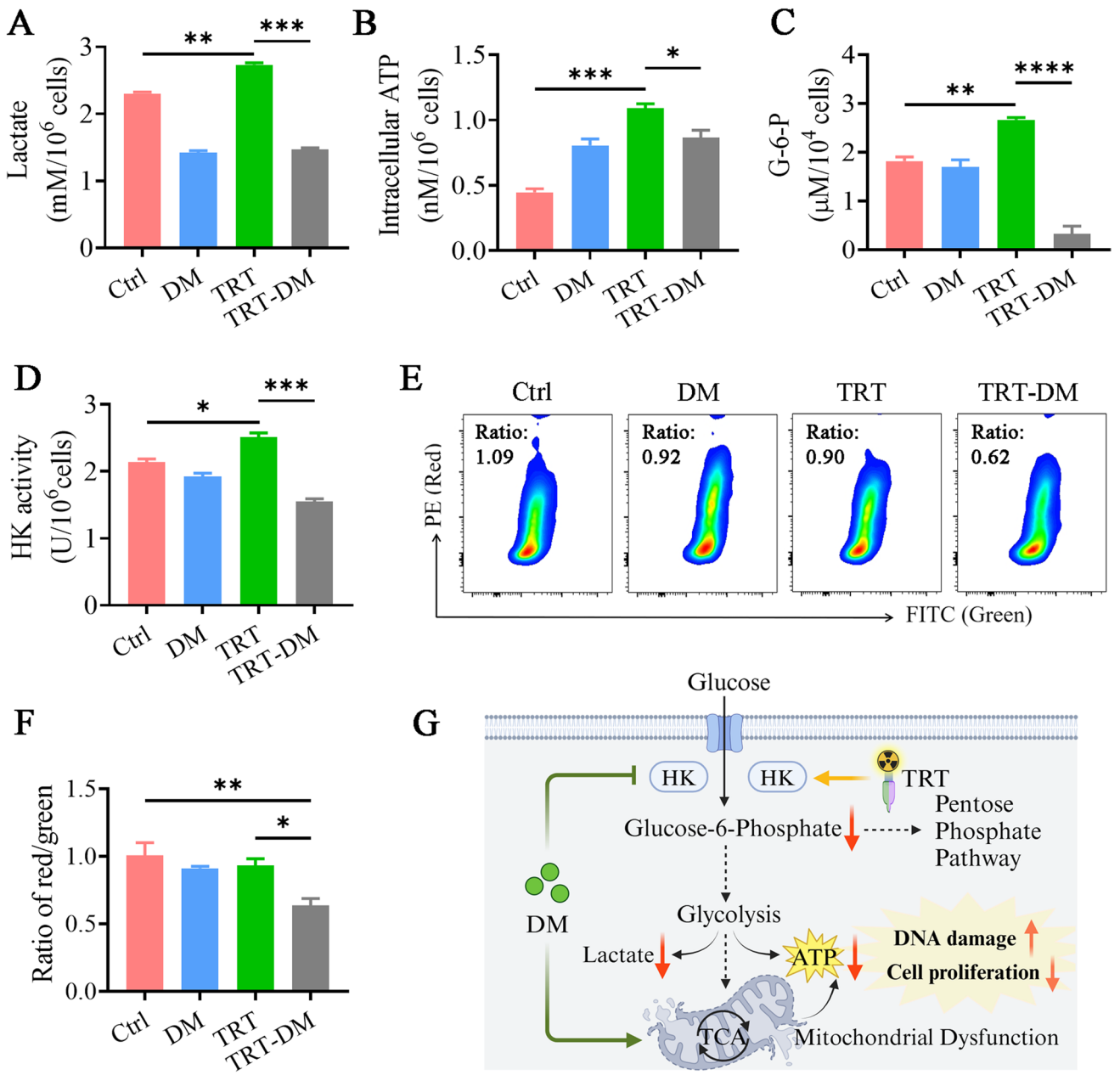

Fig. 2 Metabolic mechanisms of DM in enhancing TRT sensitivity. Changes of glucose metabolites in RM1-hPSMA cells treated with TRT, DM and TRT-DM for 48 h: (**A**) lactate concentration, (**B**) ATP content, (**C**) G-6-P concentration, and (**D**) HK activity. Flow cytometry analysis of mitochondrial membrane potential using the JC-1 probe. (**E**) Representative flow plots of aggregate (Red) and monomer (Green) proportions and (**F**) the corresponding ratios of red fluorescence to green fluorescence of RM1-hPSMA cells with different treatments. (**G**) Schematic diagram of the regulatory effect of DM on TRT-induced glucose metabolism (TRT: 50 μCi/mL, DM: 5 mM, n = 3). Data are presented as mean ± SEM. The p values in **A-D** and **F** were calculated by one-way ANOVA with Tukey's multiple comparison test; * $p < 0.05$, ** $p < 0.01$, *** $p < 0.001$, **** $p < 0.0001$

In vitro *cytotoxicity*

The cytotoxicity of ^{177}Lu-S1R/PSMA-P (TRT) and D-mannose (DM) was assessed using the MTT assay. RM1-hPSMA cells (3×10^3/well) were seeded in 96-well plates and incubated for 24 h. Cells were then treated with varying doses of TRT and DM for 48 h. After that, 10 μL of MTT reagent (5 mg/mL) was added, and cells were incubated for 4 h. The medium was replaced with 150 μL of DMSO to dissolve the formazan crystals, and absorbance at 570 nm was measured to assess cell viability.

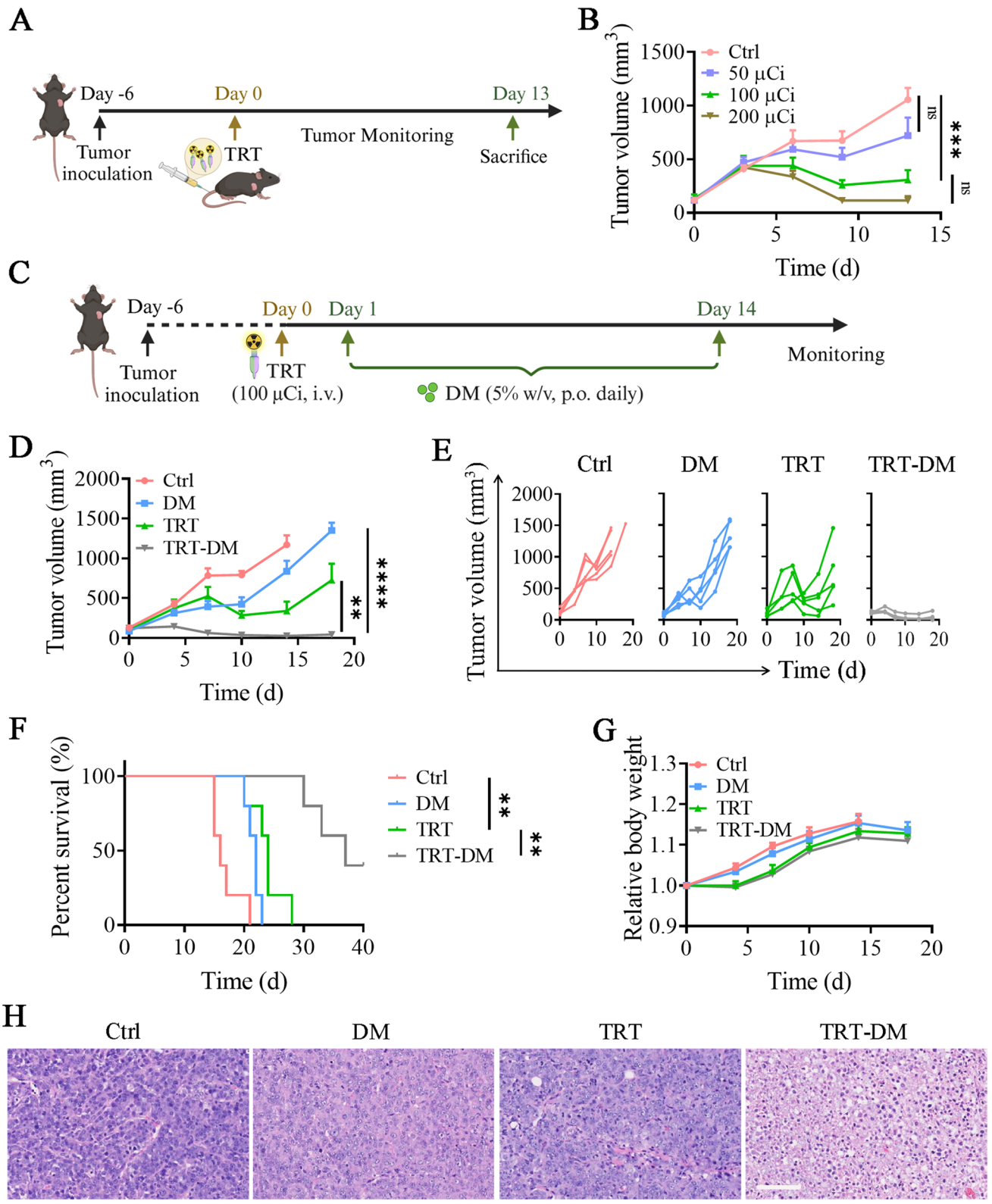

Fig. 3 DM enhanced the in vivo therapeutic effect of TRT in RM1-hPSMA tumor-bearing mice. (**A**) Treatment schedule for studying the efficacy of various TRT doses and (**B**) tumor growth curves. (**C**) Treatment regimens for TRT-DM for D-H. (**D**) Tumor growth curves, (**E**) individual tumor growth curves, (**F**) survival curves, and (**G**) relative average body weight of mice (n = 5). (**H**) Typical hematoxylin–eosin (H&E, scale bar: 80 μm) of RM1-hPSMA tumors. Data are presented as mean ± SEM. The p values in **B** and **D** were calculated by one-way ANOVA with Tukey's multiple comparison test; ** $p < 0.01$, *** $p < 0.001$, **** $p < 0.0001$; ns, no significance

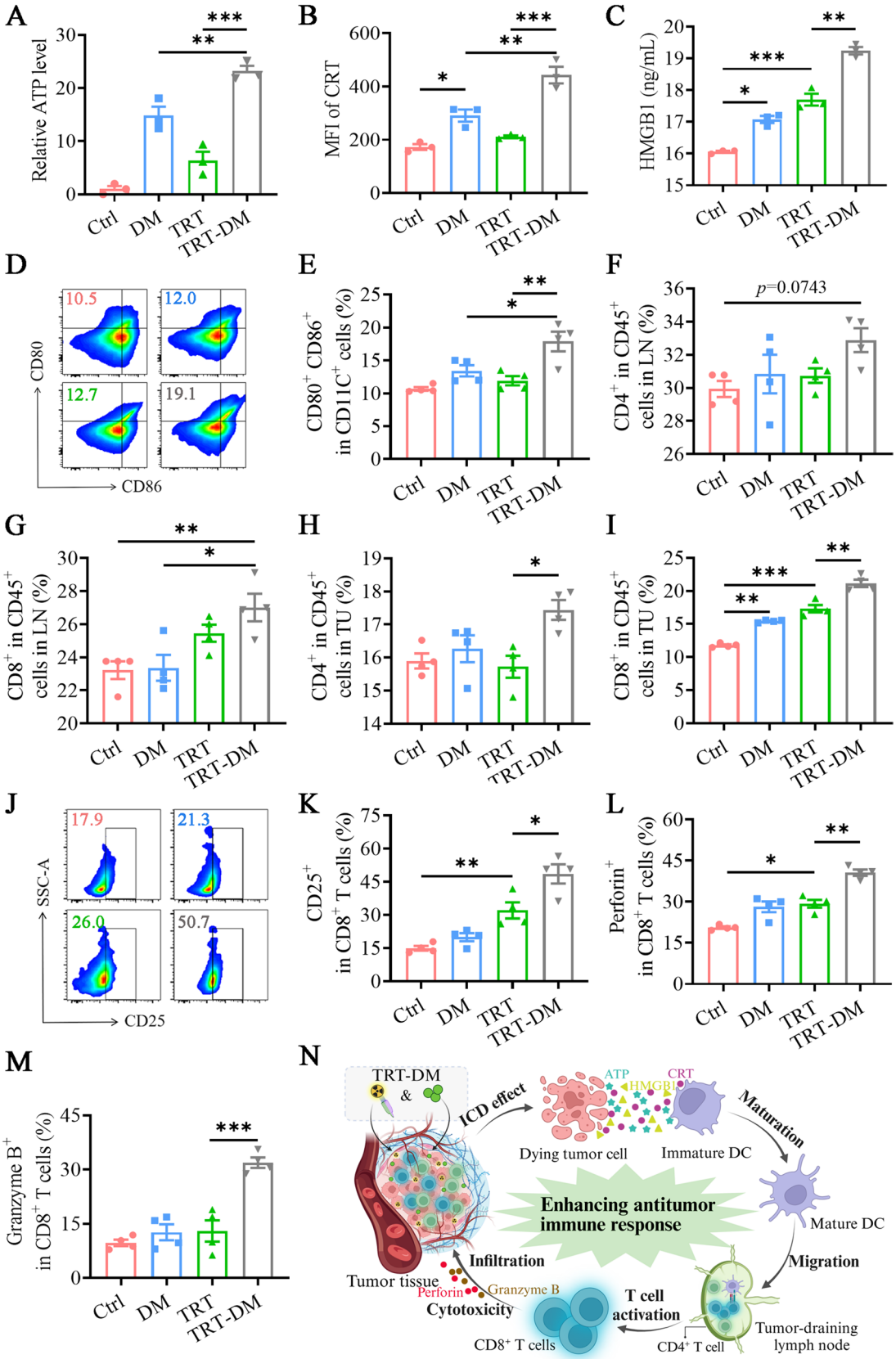
A
Relative ATP level
B
MFI of CRT
C
HMGB1 (ng/mL)
D
10.5
12.0
12.7
19.1
CD80
CD86
E
CD80+ CD86+ in CD11C+ cells (%)
F
p=0.0743
CD4+ in CD45+ cells in LN (%)
G
CD8+ in CD45+ cells in LN (%)
H
CD4+ in CD45+ cells in TU (%)
I
CD8+ in CD45+ cells in TU (%)
J
17.9
21.3
26.0
50.7
SSC-A
CD25
K
CD25+ in CD8+ T cells (%)
L
Perforin+ in CD8+ T cells (%)
M
Granzyme B+ in CD8+ T cells (%)
Ctrl
DM
TRT
TRT-DM
N
TRT-DM
&
ICD effect
ATP
HMGB1
CRT
Dying tumor cell
Immature DC
Maturation
Mature DC
Migration
Enhancing antitumor immune response
Infiltration
Tumor tissue
Perforin
Granzyme B
Cytotoxicity
T cell activation
CD8+ T cells
CD4+ T cell
Tumor-draining lymph node

◂**Fig. 4** DM enhanced the anti-tumor immune response of TRT. ICD markers (**A**) ATP, (**B**) CRT, and (**C**) HMGB1 in RM1-hPSMA cells subjected to TRT, DM, and TRT-DM for 48 h (n = 3). (**D-G**) Analyses of tumor-draining lymph nodes (TDLNs). (**D**) Flow cytometric plots and (**E**) semi-quantitative analysis of mDCs ($CD11c^+$ $CD80^+$ $CD86^+$), as well as the populations of (**F**) $CD4^+$ and (**G**) $CD8^+$ T cells in TDLNs of RM1-hPSMA tumor-bearing mice (n = 4). (**H-M**) Analyses of immune cells in the tumor tissues. Populations of (**H**) $CD4^+$ and (**I**) $CD8^+$ T cells in tumors (n = 4). (**J**) Representative flow cytometry plots and (**K**) semi-quantitative analysis of activated $CD8^+$ T cells ($CD8^+$ $CD25^+$), along with (**L-M**) cytotoxic $CD8^+$ T cells ($CD8^+$ $Perforin^+$/$Granzyme\ B^+$) within tumors (n = 4). (**N**) Illustration depicting the enhancement of the anti-tumor immune response by TRT-DM. Data are presented as mean ± SEM. The p values in **A-C**, **E-I** and **K-M** were calculated by one-way ANOVA with Tukey's multiple comparison test; * $p < 0.05$, ** $p < 0.01$, *** $p < 0.001$

Cell cycle analysis

RM1-hPSMA cells (3×10^5/well) were seeded in 6-well plates and treated with TRT, DM, or TRT-DM for 48 h. After treatment, cells were fixed in 70% ethanol at 4 ℃ for 24 h. Fixed cells were then incubated with RNase A (100 mg/L) and Propidium Iodide (50 μg/mL) for 30 min. Cell cycle distribution was analyzed using flow cytometry and Modifit software.

Immunofluorescence staining analysis of γ-H2AX

To assess the level of DNA double-strand breaks (DSBs) in RM1-hPSMA cells, the cells (5×10^4/well) were seeded in 12-well plates and treated with TRT (50 μCi/mL), DM (5 mM), or TRT-DM for 48 h. Cells were fixed, washed, and blocked, then incubated overnight with a rabbit monoclonal anti-γ-H2AX antibody. After incubation with a Cy3-labeled secondary antibody for 1 h at 4 ℃, nuclei were stained with DAPI. Staining was observed using a confocal fluorescence microscope (Olympus).

Cell metabolism experiments

RM1-hPSMA cells (3×10^5/well) were cultured in 6-well plates for attachment, followed by treatment with TRT (50 μCi/mL), DM (5 mM), or TRT-DM for 48 h. **Intracellular lactate content detection:** After treatment, cells were collected, lysed, and centrifuged to obtain the supernatant. Lactate content was measured using a lactic acid assay kit according to the manufacturer's instructions. **ATP content evaluation:** Post-treatment, cells were lysed using ice-cold lysis buffer, and the ATP content in the supernatant was quantified using the Enhanced ATP Detection Kit. **HK activity assay:** Cells were treated as described and then sonicated for 15 min. The supernatant was centrifuged, and HK activity was measured by mixing with preheated HK reagent. Absorbance at 340 nm was recorded initially and after 5 min at 37 ℃, and the activity was calculated using the HK Activity Assay Kit. **G-6-P content test:** After treatment, cells were collected, lysed with cold G-6-P extract, and centrifuged. The supernatant was incubated with G-6-P detection reagent, and absorbance was measured at 450 nm to determine G-6-P concentration using a standard curve. **Mitochondrial membrane potential assay:** After 48 h of treatment, cells were washed with PBS, stained with JC-1 probe for 20 min in the dark, then centrifuged, washed twice with cold JC-1 buffer, and resuspended. Mitochondrial membrane potential was assessed by flow cytometry.

Immunogenic cell death (ICD) effect assessment

RM1-hPSMA cells (8×10^4/well) were seeded in 12-well plates and treated with TRT (50 μCi/mL), DM (5 mM), or TRT-DM. For ATP and HMGB1 content, supernatants were collected and analyzed using the Enhanced ATP Detection Kit and mouse HMGB1 ELISA Kit, respectively, with results measured by a microplate reader (BioTek) and GraphPad Prism. For CRT expression, cells were digested, centrifuged, and stained with CRT antibody and Alexa Fluor 647-labeled secondary antibody. After washing, cells were resuspended in PBS, and CRT expression was assessed by flow cytometry.

Establishment and treatment of RM1-hPSMA tumor-bearing mice

All animal procedures were performed in accordance with the Guidelines for Care and Use of Laboratory Animals of Soochow University (P.R. China) and approved by the Animal Ethics Committee of Soochow University. To simulate prostate cancer heterogeneity, RM1 and RM1-hPSMA cells were digested during logarithmic growth and mixed at a ratio of 70% RM1-hPSMA to 30% RM1. A 100 μL suspension containing 2.5×10^6 cells was injected into the shaved subcutaneous region of the right shoulder of C57BL/6 J mice to establish the RM1-hPSMA tumor model.

To determine the optimal TRT dose for combination therapy, RM1-hPSMA tumor-bearing mice (100–150 mm^3) were assigned to four groups (n = 5): (1) Control (untreated), (2) TRT at 50 μCi, (3) TRT at 100 μCi, and (4) TRT at 200 μCi. Mice received the respective TRT dose via tail vein injection on day 0. Tumor volume was monitored every three days to assess efficacy, with tumor volume calculated as tumor volume $= L \times W^2/2$, where L and W are tumor length and width.

To evaluate the sensitizing effect of DM, RM1-hPSMA tumor-bearing mice (100–150 mm^3) were treated as follows

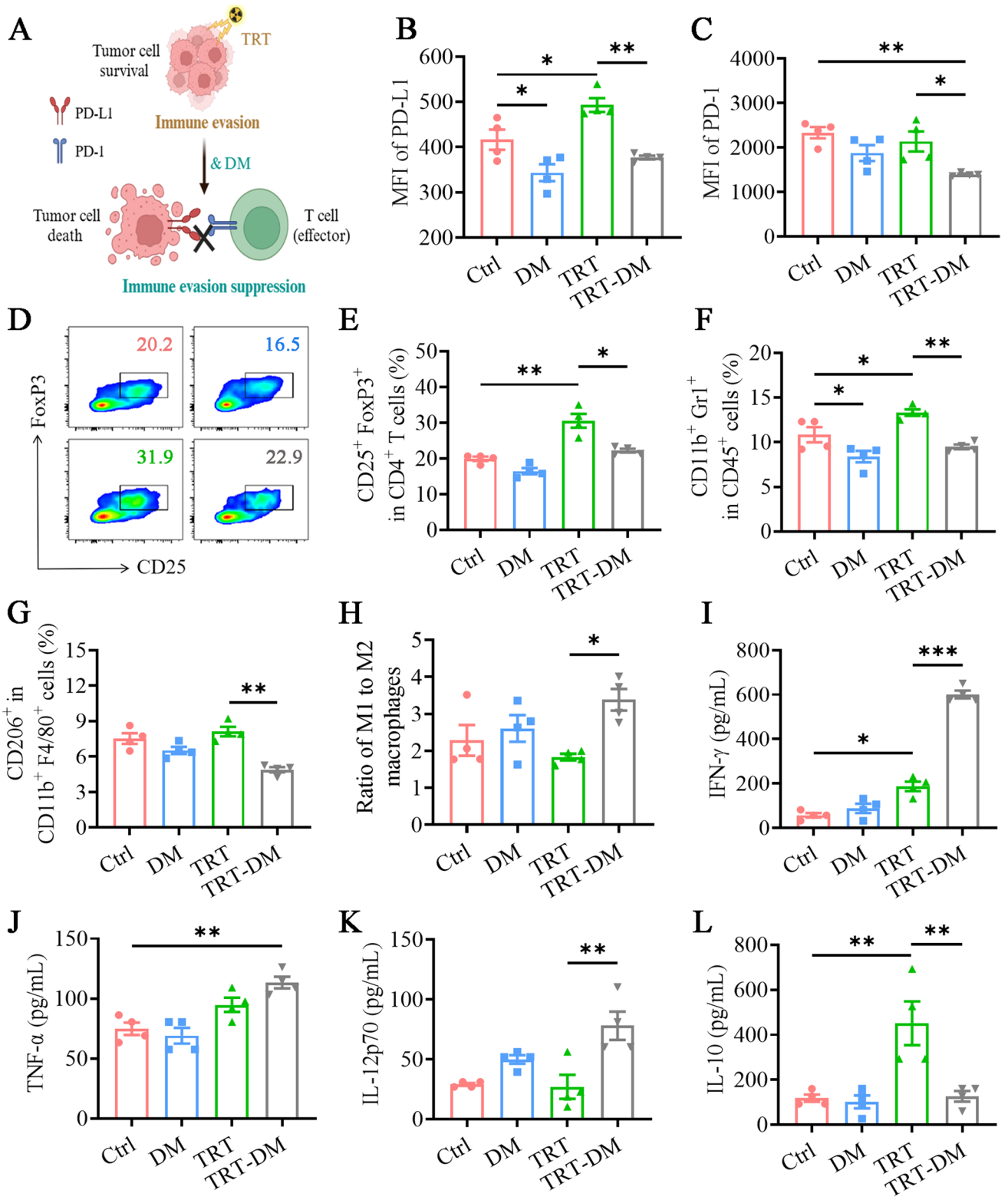

(n = 6): (1) Control, (2) DM (5% w/v), (3) TRT at 100 μCi, and (4) TRT-DM. On day 0, groups (3) and (4) received TRT through intravenous tail injection, while DM was administered ad libitum in drinking water at a concentration of 5% w/v (10 g DM dissolved in 200 mL water), starting from day 1 and continued for two weeks. Tumor volume and body weight were recorded every three days. On day 2 post-treatment, one mouse from each group was dissected, and tumor

◂**Fig. 5** Immunological mechanism study of DM-potentiated TRT. (**A**) Schematic illustration of DM inhibiting immune evasion induced by TRT in RM1-hPSMA tumor-bearing mice. (**B-H**) Analyses of immune cells in the tumor tissues. (**B**) PD-L1 expression levels on tumor cells ($CD45^-$) and (**C**) PD-1 expression on $CD8^+$ T cells within the TME. (**D**) Representative flow cytometric plots and (**E**) semi-quantitative analysis of Tregs ($CD4^+$ $CD25^+$ $FoxP3^+$) in tumors. Populations of (**F**) MDSCs ($CD11b^+$ $Gr1^+$), (**G**) M2-type macrophages ($CD11b^+$ $F4/80^+$ $CD206^+$), and (**H**) ratios of M1-type macrophages ($CD11b^+$ $F4/80^+$ $CD86^+$) to M2-type macrophages. (**I-L**) Quantitative analyses of cytokines in serum by ELISA (n = 4). (**I**) IFN-γ, (**J**) TNF-α, (**K**) IL-12p70, and (**L**) IL-10. Data are presented as mean ± SEM. The p values in **B**, **C** and **E-L** were calculated by one-way ANOVA with Tukey's multiple comparison test; * $p < 0.05$, ** $p < 0.01$, *** $p < 0.001$

tissues were analyzed via H&E and immunofluorescence (CD8, CD206) staining. Mice with tumors exceeding 2000 mm^3 or > 15% weight loss were euthanized.

Remodeling of the immune microenvironment in vivo

To assess the immune effects of TRT-DM, RM1-hPSMA tumor-bearing mice (n = 4) with tumor volumes of 300 mm^3 were treated as previously described. On day 2 post-treatment, blood was collected for immunological analysis. Serum was obtained via centrifugation and used to quantify IFN-γ, TNF-α, IL-10, and IL-12p70 by ELISA. Mice were then euthanized, and lymph nodes, spleens, and tumor tissues were harvested and processed into single-cell suspensions. Red blood cells were lysed, and live cells were identified using Zombie NIR solution. Surface antigens were stained following Fc receptor blocking with CD16/32 antibodies. For intracellular and nuclear staining, cells were fixed and permeabilized using the Foxp3/Transcription Factor Staining Buffer Set. Flow cytometry was used to analyze various immune cell populations, including T cells ($CD45^+$ $CD3^+$ $CD4^+$ $CD8^+$ $CD25^+$), dendritic cells (DCs; $CD11c^+$ $MHCII^+$ $CD103^+$/$CD80^+$ $CD86^+$), myeloid-derived suppressor cells (MDSCs; $CD45^+$ $CD11b^+$ $Gr1^+$), macrophages ($CD11b^+$ $F4/80^+$ $CD86^+$ $CD206^+$), regulatory T cells (Tregs; $CD45^+$ $CD3^+$ $CD4^+$ $CD25^+$ $FoxP3^+$), PD-1^+ T cells ($CD45^+$ $CD3^+$ $CD8^+$ PD-1^+), and Granzyme B^+/Perforin$^+$ T cells ($CD45^+$ $CD3^+$ $CD8^+$ Granzyme B^+ Perforin$^+$) (Table S1).

Antitumor effect on LNCaP Clone FGC tumor-bearing mice

LNCaP Clone FGC tumor-bearing mice (200 mm^3) were randomly assigned to four groups (n = 5): (1) Control; (2) DM: 20% w/v DM via gavage, with 5% w/v DM in drinking water; (3) TRT: 100 μCi; (4) TRT-DM. On day 0, TRT was administered intravenously to groups (3) and (4). From day 1, groups (2) and (4) received 5% w/v DM in water for 14 days, and starting on day 2, groups (2) and (4) were gavaged with 20% w/v DM every two days (five doses total). Tumor volume and body weight were measured every three days. After treatment, blood samples were collected for routine analysis. Mice with tumor volumes > 2000 mm^3 or > 15% weight loss were euthanized.

Statistical analysis

Data were presented as mean ± SEM (n ≥ 3) and analyzed using a two-tailed Student's t-test for two-group comparisons, and one-way ANOVA for multiple group differences (GraphPad Prism 8.0.2). Survival rates were analyzed by the Kaplan-Meier method with Log-rank test comparisons. Significance thresholds were set at * $p < 0.05$, ** $p < 0.01$, *** $p < 0.001$, **** $p < 0.0001$.

Results and discussion

D-mannose sensitizes TRT in vitro

We conducted a systematic study on the radio-sensitizing effect of D-mannose (DM) in RM1-hPSMA prostate cancer cells. MTT assays showed that when treated with only ^{177}Lu-S1R/PSMA-P (TRT), even at a high dose (50 μCi/mL), cells maintained round 84% viability (Fig. 1A), demonstrating the inherent resistance of RM1-hPSMA cells to TRT. DM used alone at concentrations up to 5 mM did not cause obvious toxicity (Fig. 1B), indicating its good safety profile. TRT (5 or 50 μCi/mL) combined with DM, however, significantly elevated cell inhibition (Fig. 1C). Clonogenic assays showed markedly reduced colonies in the TRT-DM group (Fig. 1D). The sensitizing effect of DM was also reflected in the regulation of the cell cycle and the exacerbation of DNA damage. The cell cycle analysis demonstrated that TRT-DM significantly increased the accumulation of cells in the G2/M phase (Fig. 1E, F), indicating increased DNA damage [32]. The immunofluorescence staining visualized that TRT-DM induced marked increase of γ-H2AX signal (Fig. 1G), supporting an increased DNA double-strand break. Figure 1H shows that DM boosted the apoptosis rate, particularly late apoptosis, caused by TRT. These data corroborate that DM effectively sensitizes RM1-hPSMA cells to TRT.

D-mannose sensitizes TRT by inhibiting glucose metabolism

A prominent characteristic of prostate cancer is the reprogramming of glucose metabolism, primarily manifested by enhanced glycolysis and accelerated energy metabolism [33]. Although radiotherapy can effectively kill tumor cells, it may enhance the tumor cells' radiation resistance by

intensifying glycolysis and even activating other metabolic pathways such as the pentose phosphate pathway (PPP) [14]. Here, we assessed the role of DM in regulating the glycolytic changes induced by TRT. TRT was shown to significantly increase the lactate levels, a marker of glycolytic activity, which was markedly reduced by DM (Fig. 2A), suggesting its strong inhibitory effect on glycolysis. Similarly, DM also reduced ATP levels (Fig. 2B) and glucose-6-phosphate (G-6-P) levels caused by TRT (Fig. 2C). The hexokinase (HK) activity and mitochondrial membrane potential (MMP) assays revealed that DM significantly downregulated HK activity (Fig. 2D) and the aggregate-to-monomer ratio (Fig. 2E, F), respectively, indicating a strong inhibition of the initiating enzyme of glucose metabolism and substantial mitochondrial dysfunction, which could be a key pathway in further weakening glucose metabolism [34].

Hence, DM comprehensively inhibits metabolic pathways such as glycolysis, PPP, and OXPHOS by regulating key enzyme activities and damaging mitochondrial function, weakening the metabolic enhancement effect induced by TRT (Fig. 2G). This intervention not only restricts the energy supply and proliferative capacity of tumor cells but also impedes DNA damage repair [11, 35]. It is acknowledged, nevertheless, that our results regarding the suppression of glucose metabolism were derived solely from in vitro experiments, and there is lack of in vivo validation (e.g., via FDG-PET imaging) using tumor-bearing models.

D-mannose enhances the TRT of murine prostate cancer in vivo

The radio-sensitization effect of DM was studied in murine RM1-hPSMA tumor model. We firstly investigated TRT with different doses of ^{177}Lu-S1R/PSMA-P by monitoring tumor volume changes over 13 days (Fig. 3A). The results displayed that 100 μCi of TRT significantly suppressed tumor growth, whereas doubling the dose to 200 μCi did not induce significant difference in tumor inhibition (Fig. 3B), in line with radiation resistance. In the following, 100 μCi was selected as an optimal TRT dose for subsequent experiments and DM was given daily for two weeks (Fig. 3C). Tumor growth curves revealed that DM while alone had trivial impact on tumor growth significantly enhanced TRT of RM1-hPSMA tumor (Fig. 3D, E). In accordance, TRT-DM greatly prolonged the median survival time to 37 days, which contrasts with 22 and 24 days for DM and TRT single treatments, respectively (Fig. 3F). All groups had little body weight loss (Fig. 3G), indicating a good safety of all treatments. H&E staining of tumor tissues revealed a more pronounced apoptosis and necrosis by TRT-DM (Fig. 3H). The above results confirm that DM can significantly enhance the radiosensitivity of prostate tumor to TRT without causing apparent side effects.

D-mannose-TRT induces strong anti-tumor immune response

The β-particles emitted by TRT can induce ICD of tumor cells [36]. Interestingly, our results showed that DM significantly increased ATP, CRT and HMGB1 levels by TRT (Fig. 4A-C), suggesting that TRT-DM triggers stronger anti-tumor immune response. We further found that TRT-DM induced significantly more mature dendritic cells (mDCs, $CD80^+$ $CD86^+$) (Fig. 4D, E) and $CD103^+$ DCs (cDC1, $CD103^+$ $MHCII^+$) (Figure S1) in the tumor-draining lymph nodes (TDLNs), which are the crucial sites for the initiation of adaptive immune responses [37]. In accordance, TRT-DM promoted activation of $CD4^+$ T cells in TDLNs and significantly increased the proportion of $CD8^+$ T cells (Fig. 4F-G), similar to previous report [38]. TRT-DM was further shown to induce significantly more T cells ($CD3^+$, $CD4^+$, $CD8^+$) in the spleen and peripheral blood (**Figure S**2), signifying systemic immune activation.

The analysis of tumor microenvironment (TME) revealed that TRT-DM led to significantly increased infiltration of $CD4^+$ T cells and $CD8^+$ T cells (Fig. 4H, I and **S**3). Although TRT alone elevated the activation state ($CD25^+$) of $CD8^+$ T cells and their secretion of perforin, its effect on granzyme B was limited. In comparison, TRT-DM significantly upregulated the expression of CD25, perforin, and particularly granzyme B (Fig. 4J-M), thereby enhancing the cytotoxicity of $CD8^+$ T cells [39]. This enhancement may be associated with DM's inhibition of tumor glycolysis, reduction of lactate accumulation, and alleviation of metabolic suppression of T cells in the TME [40–42]. Hence, TRT-DM enhances the expression of ICD markers and promotes the activation and functionality of DCs and T cells (Fig. 4N).

D-mannose-TRT remodels tumor microenvironment

The TME characterized by immune suppression is a key factor contributing to the suboptimal efficacy of anti-tumor therapies, with immune checkpoint pathways playing a particularly crucial role [43] (Fig. 5A). Previous studies have indicated that ^{177}Lu-based TRT would induce PD-L1 upregulation on tumor cells [44, 45], thereby enhancing the immune evasion of tumor cells. Interestingly, our results demonstrated that DM significantly reduced PD-L1 protein and mRNA expression levels induced by TRT in RM1-hPSMA cells (**Figure S**4, 5). The in vivo experiments revealed that in contrast to marked upregulation of PD-L1 on tumor cells ($CD45^-$) by TRT alone, TRT-DM reduced PD-L1 expression (Fig. 5B). Moreover, TRT-DM significantly reduced PD-1 expression on tumor-infiltrating $CD8^+$ T cells (Fig. 5C), suggesting that DM may effectively mitigate TRT-induced immune escape.

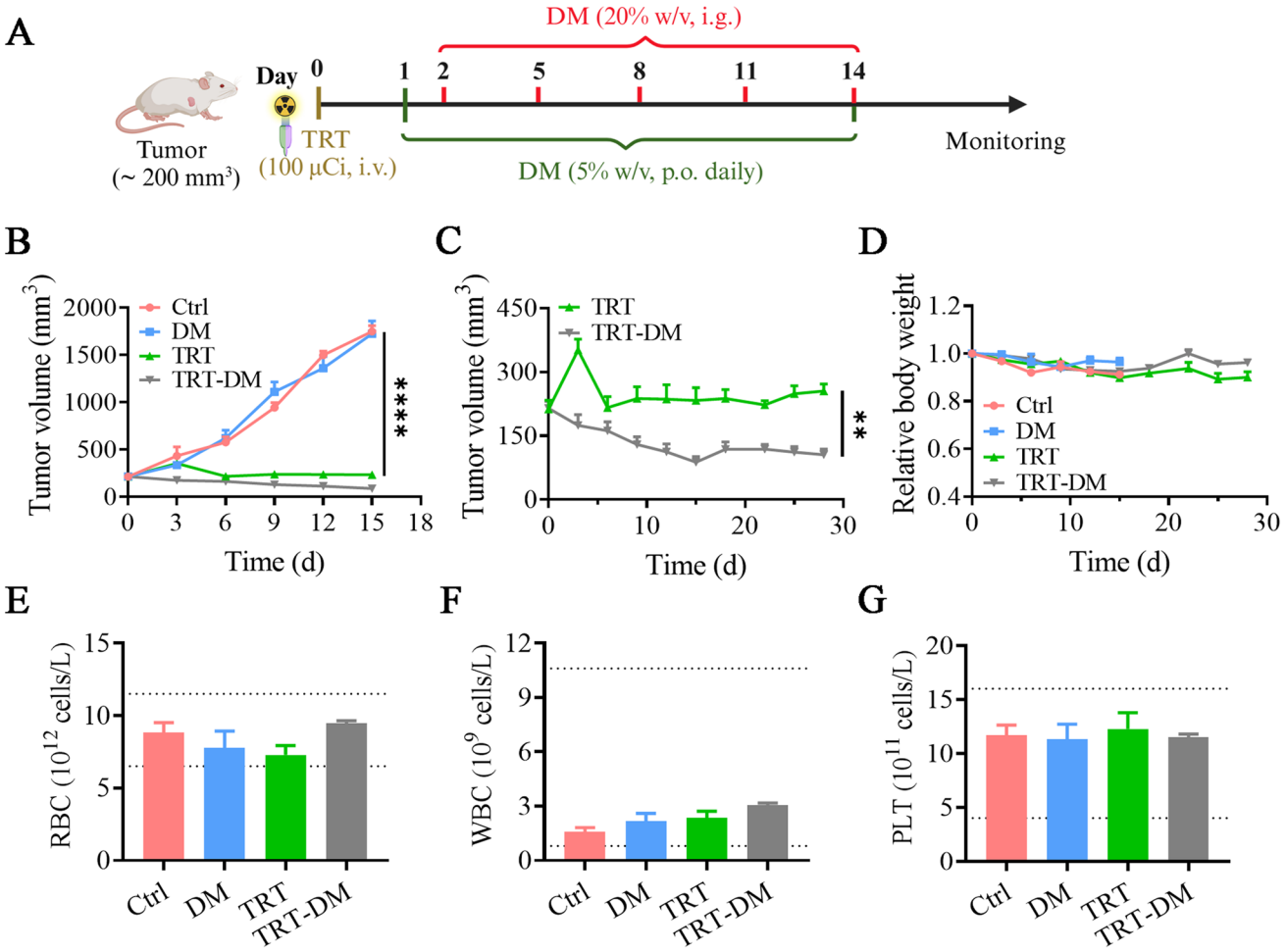

Fig. 6 DM enhanced the in vivo therapeutic effect of TRT in LNCaP Clone FGC tumor-bearing mice (n = 5). (**A**) Treatment regimen for TRT combined with DM. (**B**) Tumor growth curve, (**C**) tumor growth curves of TRT and TRT-DM groups, (**D**) relative body weights of the mice. Blood routine analysis of (**E**) red blood cells (RBC), (**F**) white blood cells (WBC), and (**G**) platelets (PLT). Data are presented as mean ± SEM. The p values in **B** and **C** were calculated using a two-tailed Student's *t*-test; **p < 0.01, ****p < 0.0001

In addition to PD-L1 and PD-1, radiation might also enhance immune suppression by increasing the infiltration of other immunosuppressive cells such as myeloid-derived suppressor cells (MDSCs), tumor-associated macrophages (TAMs), and regulatory T cells (Tregs) within the tumor [46]. We found that unlike a significant increase of Tregs by TRT, TRT-DM effectively reduced Tregs (Fig. 5D, E). This helps restore the balance between effector T cells and Tregs, thereby reducing radiation resistance [47]. Similarly, the number of MDSCs also increased after TRT, which may be related to the upregulation of lactate [13, 48]. DM significantly reduced the number of MDSCs by TRT (Fig. 5F). Additionally, TRT-DM reduced the proportion of pro-tumoral M2 macrophages and increased the ratio of anti-tumoral M1-type macrophages (M1M) to M2-type macrophages (M2M) (Fig. 5G, H and **S**3), enhancing the anti-tumor immune response [49, 50]. Further investigation through ELISA revealed that compared to TRT alone, TRT-DM significantly enhanced the secretion of anti-tumor cytokines such as IFN-γ, TNF-α, and IL-12p70, while significantly reducing the secretion of the pro-tumoral cytokine IL-10 (Fig. 5I-L), which suggests that DM can also improve the systemic immune microenvironment by regulating the secretion of key immune cytokines [51]. Hence, DM effectively reshapes the immunosuppressive microenvironment induced by TRT by blocking the PD-1/PD-L1 pathway and regulating the infiltration of immunosuppressive cells.

D-mannose-TRT effectively inhibits human prostate cancer xenografts in mice

We further studied the radio-sensitization effect of DM in LNCaP Clone FGC human prostate tumor model. NCG mice with severe immunodeficiency would limit the immune modulation ability of DM. **Figure S**6 shows that DM exerted

minimal toxic effects on LNCaP Clone FGC cells. The dosing regimen of DM was given in Fig. 6A. The results showed DM had no any inhibitory effect and tumor grew rapidly to 1800 mm^3 in day 15 (Fig. 6B). In contrast, TRT in particular when combined with DM effectively inhibited tumor growth, in which tumor volumes of approximately 250 mm^3 and 100 mm^3 were observed for TRT and TRT-DM, respectively, on day 28 (Fig. 6C), supporting radio-sensitization effect of DM. It is interesting to note that DM was much less effective in boosting the tumor inhibition in the xenograft model than in the syngeneic model (Fig. 6B *versus* Fig. 3D), supporting that besides enhancing radiosensitivity, reshaping the immune tumor microenvironment has significantly contributed to the observed therapeutic effects of DM in TRT for immunocompetent mice. Figure 6D shows that mice body weights remained within normal ranges. The complete blood count analyses indicated that red blood cell (RBC), white blood cell (WBC), and platelet (PLT) counts for all treatment groups were within normal limits (Fig. 6E-G), suggesting absence of hematological toxicity and confirming good safety of TRT-DM.

Conclusion

We have demonstrated that D-mannose (DM) can effectively sensitize TRT of malignant prostate tumor with ^{177}Lu-S1R/PSMA-P by suppressing the TRT-induced enhancement of glucose metabolism. Interestingly, DM has not only increased DNA damage by TRT, leading to elevated apoptosis rate, but also intensifies the immunogenic cell death, inhibits the TRT-induced upregulation of PD-L1 on tumor cells and PD-1 on T cells, and reduces the infiltration of immunosuppressive cells in the tumor microenvironment, thereby impairing tumor immune escape and enhancing anti-tumor immunity. TRT-DM results in synergistic treatment effects in murine RM1-hPSMA tumor model. Enhanced tumor inhibition is also observed in human LNCaP Clone FGC-bearing NCG mice. This study proves that DM is an excellent radio-sensitizer and TRT-DM has a great potential for clinical translation.

Supplementary Information The online version contains supplementary material available at https://doi.org/10.1007/s13346-025-01886-w.

Acknowledgements Not applicable.

Authors'contributions Lei Tao performed the experiments and wrote original draft; Bin Xu and Juan Sun helped the animal experiments and data analysis; Jiangtao Yang supervised the daily work; Fenghua Meng reviewed and critically revised the manuscript; Zhiyuan Zhong made conceptualization, supervised the work and revised the manuscript.

Funding This work is supported by research grants from the National Natural Science Foundation of China (NSFC52233007).

Data availability Data are available upon reasonable requirements from authors.

Not applicable.

Declarations

Ethics approval and consent to participate Not applicable.

Consent for publication Not applicable.

Competing interests The authors declare no competing interests.

References

1. Bray F, Laversanne M, Sung H, Ferlay J, Siegel RL, Soerjomataram I, Jemal A. Global cancer statistics 2022: GLOBOCAN estimates of incidence and mortality worldwide for 36 cancers in 185 countries. CA Cancer J Clin. 2024;74:229–63. https://doi.org/10.3322/caac.21834.
2. Rebello RJ, Oing C, Knudsen KE, Loeb S, Johnson DC, Reiter RE, Gillessen S, Van der Kwast T, Bristow RG. Prostate cancer Nat Rev Dis Primers. 2021;7:9. https://doi.org/10.1038/s41572-020-00243-0.
3. Satapathy S, Yadav MP, Ballal S, Sahoo RK, Bal C. [177Lu]Lu-PSMA-617 as first-line systemic therapy in patients with metastatic castration-resistant prostate cancer: A real-world study. Eur J Nucl Med Mol Imaging. 2024;51:2495–503. https://doi.org/10.1007/s00259-024-06677-y.
4. Tuchayi AM, Yadav S, Jiang F, Kim ST, Saelee RK, Morley A, Juarez R, Lawhn-Heath C, Wang Y, de Kouchkovsky I, Hope TA. Real-world experience with 177Lu-PSMA-617 radioligand therapy after Food and Drug Administration approval. J Nucl Med. 2024;65:735. https://doi.org/10.2967/jnumed.123.266842.
5. Sun J, Huangfu Z, Yang J, Wang G, Hu K, Gao M, Zhong Z. Imaging-guided targeted radionuclide tumor therapy: From concept to clinical translation. Adv Drug Deliv Rev. 2022;190: 114538. https://doi.org/10.1016/j.addr.2022.114538.
6. Sartor O, de Bono J, Chi KN, Fizazi K, Herrmann K, Rahbar K, Tagawa ST, Nordquist LT, Vaishampayan N, El-Haddad G, Park CH, Beer TM, Armour A, Pérez-Contreras WJ, DeSilvio M, Kpamegan E, Gericke G, Messmann RA, Morris MJ, Krause BJ. Lutetium-177-PSMA-617 for metastatic castration-resistant prostate cancer. N Engl J Med. 2021;385:1091–103. https://doi.org/10.1056/NEJMoa2107322.
7. Hofman MS, Violet J, Hicks RJ, Ferdinandus J, Thang SP, Akhurst T, Iravani A, Kong G, Ravi Kumar A, Murphy DG, Eu P, Jackson P, Scalzo M, Williams SG, Sandhu S. [(177)Lu]-PSMA-617 radionuclide treatment in patients with metastatic castration-resistant prostate cancer (LuPSMA trial): A single-centre, single-arm, phase 2 study. Lancet Oncol. 2018;19:825–33. https://doi.org/10.1016/S1470-2045(18)30198-0.
8. Hofman M S, Emmett L, Sandhu S, Iravani A, Joshua A M, Goh J C, Pattison D A, Tan T H, Kirkwood I D, Ng S, Francis R J, Gedye C, Rutherford N K, Weickhardt A, Scott A M, Lee S T, Kwan E M, Azad A A, Ramdave S, Redfern A D, Macdonald W, Guminski A, Hsiao E, Chua W, Lin P, Zhang A Y, McJannett M M, Stockler M R, Violet J A, Williams S G, Martin A J, Davis I D, Thera P T I, the A, New Zealand U, Prostate Cancer Trials G. [(177)Lu]Lu-PSMA-617 versus cabazitaxel in patients with metastatic castration-resistant prostate cancer (TheraP): A randomised, open-label, phase 2 trial. Lancet. 2021;397:797–804. https://doi.org/10.1016/S0140-6736(21)00237-3.

9. Pathmanandavel S, Crumbaker M, Nguyen A, Yam AO, Wilson P, Niman R, Ayers M, Sharma S, Eu P, Martin AJ, Stockler MR, Joshua AM, Emmett L. The prognostic value of posttreatment (68)Ga-PSMA-11 PET/CT and (18)F-FDG PET/CT in metastatic castration-resistant prostate cancer treated with (177)Lu-PSMA-617 and NOX66 in a Phase I/II trial (Lupin). J Nucl Med. 2023;64:69–74. https://doi.org/10.2967/jnumed.122.264104.
10. Ahmad F, Cherukuri MK, Choyke PL. Metabolic reprogramming in prostate cancer. Br J Cancer. 2021;125:1185–96. https://doi.org/10.1038/s41416-021-01435-5.
11. Tang L, Wei F, Wu Y, He Y, Shi L, Xiong F, Gong Z, Guo C, Li X, Deng H, Cao K, Zhou M, Xiang B, Li X, Li Y, Li G, Xiong W, Zeng Z. Role of metabolism in cancer cell radioresistance and radiosensitization methods. J Exp Clin Cancer Res. 2018;37:87. https://doi.org/10.1186/s13046-018-0758-7.
12. Cascone T, McKenzie JA, Mbofung RM, Punt S, Wang Z, Xu C, Williams LJ, Wang Z, Bristow CA, Carugo A, Peoples MD, Li L, Karpinets T, Huang L, Malu S, Creasy C, Leahey SE, Chen J, Chen Y, Pelicano H, Bernatchez C, Gopal YNV, Heffernan TP, Hu J, Wang J, Amaria RN, Garraway LA, Huang P, Yang P, Wistuba II, Woodman SE, Roszik J, Davis RE, Davies MA, Heymach JV, Hwu P, Peng W. Increased tumor glycolysis characterizes immune resistance to adoptive T cell therapy. Cell Metab. 2018;27:977–87. https://doi.org/10.1016/j.cmet.2018.02.024.
13. Yang X, Lu Y, Hang J, Zhang J, Zhang T, Huo Y, Liu J, Lai S, Luo D, Wang L, Hua R, Lin Y. Lactate-modulated immunosuppression of myeloid-derived suppressor cells contributes to the radioresistance of pancreatic cancer. Cancer Immunol Res. 2020;8:1440–51. https://doi.org/10.1158/2326-6066.CIR-20-0111.
14. Mittal A, Nenwani M, Sarangi I, Achreja A, Lawrence TS, Nagrath D. Radiotherapy-induced metabolic hallmarks in the tumor microenvironment. Trends Cancer. 2022;8:855–69. https://doi.org/10.1016/j.trecan.2022.05.005.
15. Cao L, Yang Y, Zheng Y, Cheng W, Chen M, Wang T, Mu C, Wu M, Liu B. X-ray-triggered co-release from gold nanocluster: All-in-one nanoplatforms for cancer targeted gas and radio synergistic therapy. Adv Mater. 2024;36: e2401017. https://doi.org/10.1002/adma.202401017.
16. Fu Z, Liu Z, Wang J, Deng L, Wang H, Tang W, Ni D. Interfering biosynthesis by nanoscale metal-organic frameworks for enhanced radiation therapy. Biomaterials. 2023;295: 122035. https://doi.org/10.1016/j.biomaterials.2023.122035.
17. Zhou Z, Li C, Li C, Zhou L, Tan S, Hou W, Xie C, Wang L, Shen J, Xiong W. Mitochondria-targeted nanoadjuvants induced multi-functional immune-microenvironment remodeling to sensitize tumor radio-immunotherapy. Adv Sci (Weinh). 2024;11: e2400297. https://doi.org/10.1002/advs.202400297.
18. Zhou Z, Jiang X, Yi L, Li C, Wang H, Xiong W, Li Z, Shen J. Mitochondria energy metabolism depression as novel adjuvant to sensitize radiotherapy and inhibit radiation induced-pulmonary fibrosis. Adv Sci (Weinh). 2024;11: e2401394. https://doi.org/10.1002/advs.202401394.
19. Ma X, Bi E, Lu Y, Su P, Huang C, Liu L, Wang Q, Yang M, Kalady MF, Qian J, Zhang A, Gupte AA, Hamilton DJ, Zheng C, Yi Q. Cholesterol induces CD8(+) T cell exhaustion in the tumor microenvironment. Cell Metab. 2019;30:143–56. https://doi.org/10.1016/j.cmet.2019.04.002.
20. Inamdar S, Suresh AP, Mangal JL, Ng ND, Sundem A, Wu C, Lintecum K, Thumsi A, Khodaei T, Halim M, Appel N, Jaggarapu M, Esrafili A, Yaron JR, Curtis M, Acharya AP. Rescue of dendritic cells from glycolysis inhibition improves cancer immunotherapy in mice. Nat Commun. 2023;14:5333. https://doi.org/10.1038/s41467-023-41016-z.
21. Leone RD, Powell J. Metabolism of immune cells in cancer. Nat Rev Cancer. 2020;20:516–31. https://doi.org/10.1038/s41568-020-0273-y.
22. Faubert B, Solmonson A, DeBerardinis R J. Metabolic reprogramming and cancer progression. Science. 2020;368:eaaw5473. https://doi.org/10.1126/science.aaw5473.
23. Nile DL, Rae C, Walker DJ, Waddington JC, Vincent I, Burgess K, Gaze MN, Mairs RJ, Chalmers AJ. Inhibition of glycolysis and mitochondrial respiration promotes radiosensitisation of neuroblastoma and glioma cells. Cancer Metab. 2021;9:24. https://doi.org/10.1186/s40170-021-00258-5.
24. Jin H, Liu X, Liu HX. Biological function, regulatory mechanism, and clinical application of mannose in cancer. Biochim Biophys Acta Rev Cancer. 2023;1878: 188970. https://doi.org/10.1016/j.bbcan.2023.188970.
25. Gonzalez PS, O'Prey J, Cardaci S, Barthet VJA, Sakamaki JI, Beaumatin F, Roseweir A, Gay DM, Mackay G, Malviya G, Kania E, Ritchie S, Baudot AD, Zunino B, Mrowinska A, Nixon C, Ennis D, Hoyle A, Millan D, McNeish IA, Sansom OJ, Edwards J, Ryan KM. Mannose impairs tumour growth and enhances chemotherapy. Nature. 2018;563:719–23. https://doi.org/10.1038/s41586-018-0729-3.
26. Zhang R, Yang Y, Dong W, Lin M, He J, Zhang X, Tian T, Yang Y, Chen K, Lei QY, Zhang S, Xu Y, Lv L. D-mannose facilitates immunotherapy and radiotherapy of triple-negative breast cancer via degradation of PD-L1. Proc Natl Acad Sci U S A. 2022;119: e2114851119. https://doi.org/10.1073/pnas.2114851119.
27. Yao Y, Liu W, Li J, Zhou M, Qu C, Wang K. MPI-based bioinformatic analysis and co-inhibitory therapy with mannose for oral squamous cell carcinoma. Med Oncol. 2021;38:103. https://doi.org/10.1007/s12032-021-01552-4.
28. Dong W, Lin M, Zhang R, Sun X, Li H, Liu T, Xu Y, Lv L. D-mannose targets PD-1 to lysosomal degradation and enhances T cell-mediated anti-tumor immunity. Cancer Lett. 2024;591: 216883. https://doi.org/10.1016/j.canlet.2024.216883.
29. Gill MR, Falzone N, Du Y, Vallis KA. Targeted radionuclide therapy in combined-modality regimens. Lancet Oncol. 2017;18:e414–23. https://doi.org/10.1016/S1470-2045(17)30379-0.
30. Huangfu Z, Yang J, Sun J, Xu B, Tao L, Wu J, Wang F, Wang G, Meng F, Zhong Z. PSMA and sigma-1 receptor dual-targeted peptide mediates superior radionuclide imaging and therapy of prostate cancer. J Control Release. 2024;375:767–75. https://doi.org/10.1016/j.jconrel.2024.09.040.
31. Sun J, Yang J, Guo J, Tao L, Xu B, Wang G, Meng F, Zhong Z. Dual-targeted alpha therapy mitigates prostate cancer and boosts immune checkpoint blockade therapy. J Control Release. 2025;382: 113686. https://doi.org/10.1016/j.jconrel.2025.113686.
32. Larsen BD, Benada J, Yung PYK, Bell RAV, Pappas G, Urban V, Ahlskog JK, Kuo TT, Janscak P, Megeney LA, Elsässer SJ, Bartek J, Sørensen CS. Cancer cells use self-inflicted DNA breaks to evade growth limits imposed by genotoxic stress. Science. 2022;376:476–83. https://doi.org/10.1126/science.abi6378.
33. Chen M, Xiao Z, Huang Z, Xue KY, Xia H, Zhou JW, Liao DY, Liang ZJ, Xie X, Wei QZ, Zhong L, Yang JK, Liu CD, Liu Y, Zhao SC. Glycine decarboxylase (GLDC) plays a crucial role in regulating energy metabolism, invasion, metastasis and immune escape for prostate cancer. Int J Biol Sci. 2023;19:4726–43. https://doi.org/10.7150/ijbs.85893.
34. Yang J, Chu M, Zhang Y, Qian J, Liu J, Wang M, Qiang Z, Ren J. Mito-specific nutri-hijacker synergizing mitochondrial metabolism and glycolysis intervention for enhanced antitumor bioenergetic therapy. ACS Appl Mater Interfaces. 2024;16:29902–16. https://doi.org/10.1021/acsami.4c04952.
35. Lin J, Xia L, Liang J, Han Y, Wang H, Oyang L, Tan S, Tian Y, Rao S, Chen X, Tang Y, Su M, Luo X, Wang Y, Wang H, Zhou Y, Liao Q. The roles of glucose metabolic reprogramming in chemo- and radio-resistance. J Exp Clin Cancer Res. 2019;38:218. https://doi.org/10.1186/s13046-019-1214-z.

36. Rouanet J, Benboubker V, Akil H, Hennino A, Auzeloux P, Besse S, Pereira B, Delorme S, Mansard S, D'Incan M, Degoul F, Rouzaire PO. Immune checkpoint inhibitors reverse tolerogenic mechanisms induced by melanoma targeted radionuclide therapy. Cancer Immunol Immunother. 2020;69:2075–88. https://doi.org/10.1007/s00262-020-02606-8.
37. Koukourakis MI, Giatromanolaki A. Tumor draining lymph nodes, immune response, and radiotherapy: Towards a revisal of therapeutic principles. Biochim Biophys Acta Rev Cancer. 2022;1877:188704. https://doi.org/10.1016/j.bbcan.2022.188704.
38. Qiu Y, Su Y, Xie E, Cheng H, Du J, Xu Y, Pan X, Wang Z, Chen DG, Zhu H, Greenberg PD, Li G. Mannose metabolism reshapes T cell differentiation to enhance anti-tumor immunity. Cancer Cell. 2024. https://doi.org/10.1016/j.ccell.2024.11.003.
39. Golstein P, Griffiths GM. An early history of T cell-mediated cytotoxicity. Nat Rev Immunol. 2018;18:527–35. https://doi.org/10.1038/s41577-018-0009-3.
40. Hons M, Kopf A, Hauschild R, Leithner A, Gaertner F, Abe J, Renkawitz J, Stein JV, Sixt M. Chemokines and integrins independently tune actin flow and substrate friction during intranodal migration of T cells. Nat Immunol. 2018;19:606–16. https://doi.org/10.1038/s41590-018-0109-z.
41. Deng Z, Li B, Yang M, Lu L, Shi X, Lovell JF, Zeng X, Hu W, Jin H. Irradiated microparticles suppress prostate cancer by tumor microenvironment reprogramming and ferroptosis. J Nanobiotechnology. 2024;22:225. https://doi.org/10.1186/s12951-024-02496-3.
42. Amitrano AM, Berry BJ, Lim K, Kim KD, Waugh RE, Wojtovich AP, Kim M. Optical control of CD8(+) T cell metabolism and effector functions. Front Immunol. 2021;12: 666231. https://doi.org/10.3389/fimmu.2021.666231.
43. Li X, Shao C, Shi Y, Han W. Lessons learned from the blockade of immune checkpoints in cancer immunotherapy. J Hematol Oncol. 2018;11:1–26. https://doi.org/10.1186/s13045-018-0578-4.
44. Zhao L, Pang Y, Zhou Y, Chen J, Fu H, Guo W, Xu W, Xue X, Su G, Sun L, Wu H, Zhang J, Wang Z, Lin Q, Chen X, Chen H. Antitumor efficacy and potential mechanism of FAP-targeted radioligand therapy combined with immune checkpoint blockade. Signal Transduct Target Ther. 2024;9:142. https://doi.org/10.1038/s41392-024-01853-w.
45. Shi J, Gao H, Wu Y, Luo C, Yang G, Luo Q, Jia B, Han C, Liu Z, Wang F. Nuclear imaging of PD-L1 expression promotes the synergistic antitumor efficacy of targeted radionuclide therapy and immune checkpoint blockade. Eur J Nucl Med Mol Imaging. 2024:1–15. https://doi.org/10.1007/s00259-024-06962-w.
46. Lunj S, Smith TAD, Reeves KJ, Currell F, Honeychurch J, Hoskin P, Choudhury A. Immune effects of alpha and beta radionuclides in metastatic prostate cancer. Nat Rev Urol. 2024;21:651–61. https://doi.org/10.1038/s41585-024-00924-5.
47. Mondini M, Loyher PL, Hamon P, de Thoré MG, Laviron M, Berthelot K, Clémenson C, Salomon BL, Combadière C, Deutsch E, Boissonnas A. CCR2-dependent recruitment of Tregs and monocytes following radiotherapy is associated with tnfα-mediated resistance. Cancer Immunol Res. 2019;7:376–87. https://doi.org/10.1158/2326-6066.Cir-18-0633.
48. Jiménez-Cortegana C, Galassi C, Klapp V, Gabrilovich D, Galluzzi L. Myeloid-derived suppressor cells and radiotherapy. Cancer Immunol Res. 2022;10:545–57. https://doi.org/10.1158/2326-6066.Cir-21-1105.
49. Kloosterman DJ, Akkari L. Macrophages at the interface of the co-evolving cancer ecosystem. Cell. 2023;186:1627–51. https://doi.org/10.1016/j.cell.2023.02.020.
50. Wang L, Dou X, Chen S, Yu X, Huang X, Zhang L, Chen Y, Wang J, Yang K, Bugno J, Pitroda S, Ding X, Piffko A, Si W, Chen C, Jiang H, Zhou B, Chmura SJ, Luo C, Liang HL, He C, Weichselbaum RR. YTHDF2 inhibition potentiates radiotherapy antitumor efficacy. Cancer Cell. 2023;41:1294–308. https://doi.org/10.1016/j.ccell.2023.04.019.
51. Dranoff G. Cytokines in cancer pathogenesis and cancer therapy. Nat Rev Cancer. 2004;4:11–22. https://doi.org/10.1038/nrc1252.

Publisher's Note Springer Nature remains neutral with regard to jurisdictional claims in published maps and institutional affiliations.

Springer Nature or its licensor (e.g. a society or other partner) holds exclusive rights to this article under a publishing agreement with the author(s) or other rightsholder(s); author self-archiving of the accepted manuscript version of this article is solely governed by the terms of such publishing agreement and applicable law.